J Solid State Electrochem (2012) 16:3069–3077
DOI 10.1007/s10008-012-1742-3

ORIGINAL PAPER

In vitro corrosion behavior of electrodeposited calcium phosphate coatings on Ti6Al4V substrates

R. Drevet · O. Aaboubi · H. Benhayoune

Received: 5 September 2011 / Revised: 28 March 2012 / Accepted: 2 April 2012 / Published online: 25 April 2012

Abstract Calcium phosphate coatings on titanium alloy substrates are synthesized by pulsed electrodeposition and characterized by scanning electron microscopy associated to energy dispersive X-ray spectroscopy and by X-ray diffraction. The corrosion behavior of CaP/Ti6Al4V systems and uncoated Ti6Al4V are investigated using electrochemical methods in three physiological solutions and simulated with an equivalent circuit. The results reveal that the calcium phosphate coatings act as a protective layer especially when electrodeposition is carried out in the presence of hydrogen peroxide into the electrolyte which is used to control the chemical composition of the coatings and which implies a control of the corrosion behavior of the prosthetic material.

Keywords Calcium phosphate · Coating · Titanium · Polarization · EIS · Electrodeposition

Introduction

Titanium and its alloys are widely used as implant materials in orthopedic surgery because of their good mechanical properties and their excellent biocompatibility with bone [1–4]. However, it has been reported that under in vivo conditions, the localized corrosion of the implant leads to the release of metal ions into the tissues surrounding the prosthetic material [5–7]. These metallic releases have toxic effects on the patients by the alteration of the expression of human lymphocyte-surface antigen and by the inhibition of the immune response assessed by lymphocyte proliferation [8, 9]. Calcium phosphate ceramics are usually used to coat prosthetic materials in order to make them bioactive, i.e., ability to form a real bond with the surrounding bone tissue [10–12]. Moreover, calcium phosphate coatings also modify the corrosion behavior of the implant [13–16]. Many methods are developed and used to synthesize calcium phosphate coatings onto implant surfaces, for example, plasma spray [17–19], plasma electrolytic oxidation [20], sol–gel synthesis [21–26], pulsed laser-deposition [27, 28], electrophoretic method [29–31], and electrochemical deposition [32–37]. This last method has a variety of advantages: the coating process occurs at low temperature and the chemical composition could be controlled. Different chemical compositions of the coating lead to different corrosion behaviors in physiological liquid [38].

In that framework, the present study aims in evaluating the corrosion behavior improvement of the titanium alloy Ti6Al4V when a calcium phosphate coating is electrodeposited on its surface. The originality of the electrochemical protocol developed in our lab allows synthesizing calcium phosphate coatings with various chemical compositions [39]. Two types of coatings are tested in three physiological liquids: Kokubo's simulated body fluid (SBF), Dulbecco's modified Eagle medium (DMEM), and Ringer's solution.

Experimental

Pulsed electrodeposition current

The experimental setup used for electrodeposition consists of a classical three-electrode cell: the working electrode is a Ti6Al4V substrate, the counter electrode is a high surface Pt grid, and the reference electrode is a saturated calomel electrode.

R. Drevet (✉) · O. Aaboubi · H. Benhayoune
LISM EA 4695, URCA,
21 rue Clément ADER, BP 138, 51685 Reims, Cedex 02, France
e-mail: richard.drevet@univ-reims.fr

The electrolyte is prepared by mixing a solution of 0.042 M $Ca(NO_3)_2{\cdot}4H_2O$ and 0.025 M $NH_4(H_2PO_4)$. The temperature is maintained at 60 °C. In these conditions, the pH value of the solution is 4.4.

The flat Ti6Al4V substrate has 10×10×0.6-mm size. Its surface is blasted with alumina particles to give an average roughness of 2–3 μm. Prior to coating, the substrate is etched in a mixture of nitric acid (6 % in volume) and hydrofluoric acid (3 % in volume). Then, the sample is ultrasonically cleaned in acetone and in deionized water.

Electrodeposition is performed following the procedure described in our recent work [39]. A potentiostat/galvanostat instrument (Voltalab PGP 201 Radiometer Analytical—

Table 1 Chemical composition of the physiological liquids used in this study

Components	SBF ($g\ L^{-1}$)	Ringer ($g\ L^{-1}$)	DMEM ($g\ L^{-1}$)
Inorganic salts			
NaCl	7.996	9.000	6.400
$NaHCO_3$	0.350	0.200	3.700
KCl	0.224	0.420	0.400
$K_2HPO_4{\cdot}3H_2O$	0.228	–	–
$MgCl_2{\cdot}6H_2O$	0.305	–	–
$CaCl_2$	0.278	0.480	0.264
Na_2SO_4	0.071	–	–
$MgSO_4{\cdot}7H_2O$	–	–	0.200
$NaH_2PO_4{\cdot}H_2O$	–	–	0.125
Other components			
Glucose	–	–	4.500
Sodium pyruvate	–	–	0.110
Phenol red Na			0.0159
Amino acids			
L-Arginine·HCl	–	–	0.084
L -Cystine	–	–	0.048
L-Alanyl-L-glutamine	–	–	0.868
Glycine	–	–	0.03
L-Histidine HCl·H_2O	–	–	0.042
L-Isoleucine	–	–	0.105
L-Leucine	–	–	0.105
L-Lysine·HCl	–	–	0.146
L-Methionine	–	–	0.030
L-Phenylalanine	–	–	0.066
L-Serine	–	–	0.042
L-Threonine	–	–	0.095
L-Tryptophan	–	–	0.016
L-Tyrosine	–	–	0.072
L-Valine	–	–	0.094
Vitamins			
D–calcium Pantothenate	–	–	0.004
Choline chloride	–	–	0.004
Folic acid	–	–	0.004
myo-Inositol	–	–	0.0072
Nicotinamide	–	–	0.004
Pyridoxine·HCl	–	–	0.004
Riboflavin	–	–	0.0004
Thiamine·HCl	–	–	0.004

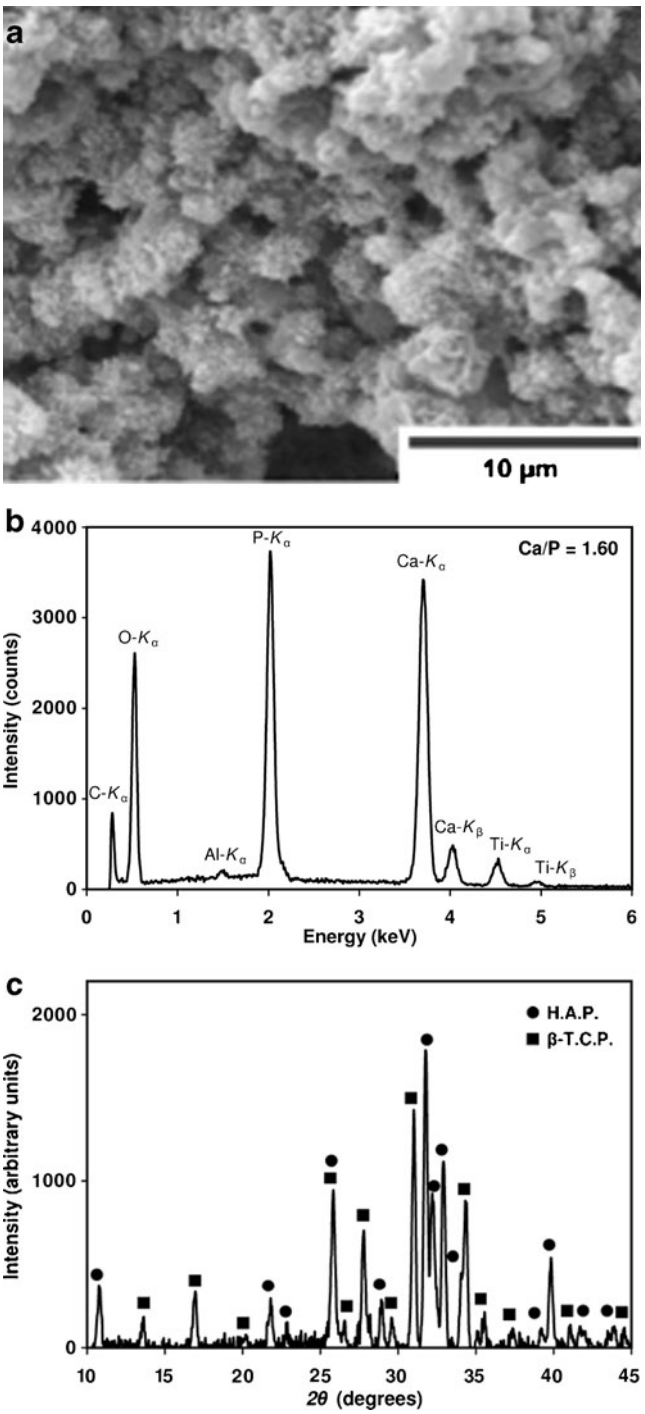

Fig. 1 Characterization of the obtained coating in pulsed electrodeposition current: **a** SEM micrograph, **b** EDXS spectrum, **c** XRD pattern after heat treatment (1,000 °C, 15 h)

VOLTAMASTER software) is used in the pulsed current mode and the deposition conditions are chosen: a deposition time t_d=1 min with a current density j_d=15 mA cm^{-2} followed by a break time t_b=2 min (j_b=0 mA cm^{-2}). The break time at zero current between two deposition times strongly reduces the H_2 bubble emission at the working electrode and allows ion concentrations to be homogenized in the solution. This process is known to produce uniform and adherent calcium phosphate coatings on titanium alloy substrate [35].

Five pulse cycles are used during deposition, which correspond to a total deposition time of 15 min.

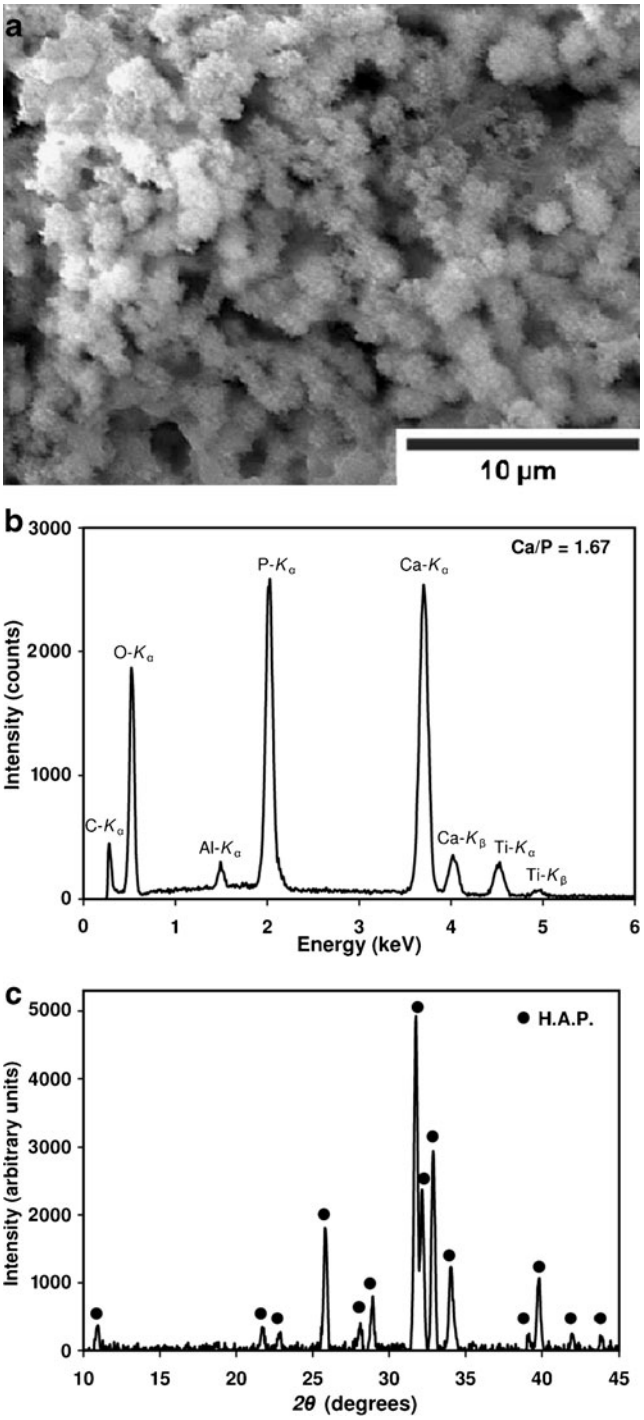

Fig. 2 Characterization of the obtained coating in pulsed electrodeposition current with 9 % H_2O_2 into electrolyte: **a** SEM micrograph, **b** EDXS spectrum, **c** XRD pattern after heat treatment (1,000 °C, 15 h)

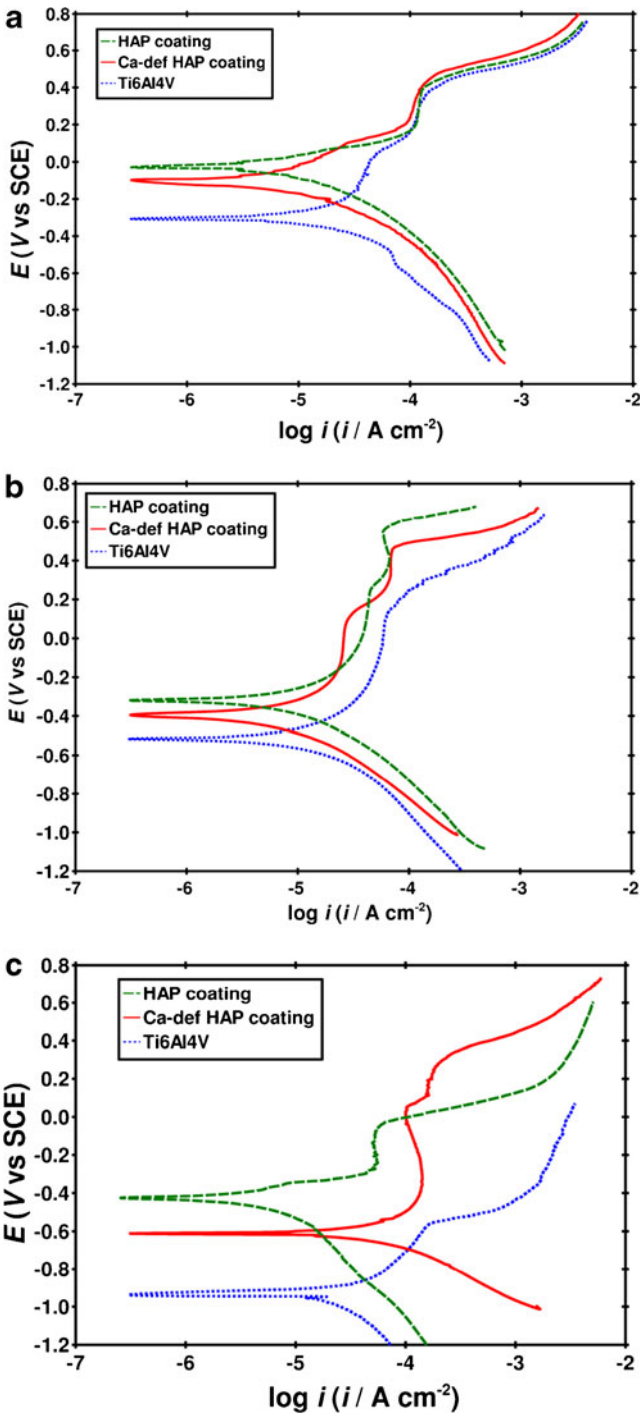

Fig. 3 Polarization curves of uncoated Ti6Al4V substrate, electrodeposited HAP coating, and electrodeposited Ca-def HAP coating. Measurements are carried out **a** in SBF, **b** in DMEM (from [42], with kind permission from Springer Science + Business Media), and **c** in Ringer's solution

In order to produce different calcium phosphate coatings, hydrogen peroxide is added to the electrolyte. In this work, the second investigated coating is synthesized by adding 9 % in volume of hydrogen peroxide (H_2O_2) into the electrolyte. The pH of the solution slightly decreases with hydrogen peroxide. Therefore the pH of the solution is adjusted to 4.4 by adding NaOH solution.

Scanning electron microscopy

The morphology of the coatings is observed with a LaB_6 electron microscope (JEOL JSM-5400LV) operating at 0–30 kV. This microscope is associated to an ultra-thin window Si(Li) detector for X-ray measurements. To avoid the charging effects, the specimens are coated with a conductive layer (Au–Pd for scanning electron microscopy (SEM) micrographs and carbon for X-ray microanalysis). The X-ray spectra are acquired at 15 kV with an acquisition time of 100 s. For the quantitative analysis, commercial software (GENESIS, Eloïse SARL, France) is used. Moreover, several measurements are carried out to calculate the mean value of the Ca/P atomic ratio.

X-ray diffraction analysis

Calcium phosphate powders are scratched from electrodeposited coatings and their phase composition is investigated using X-ray diffractometer (Bruker D8 Advance). The X-ray pattern data are collected from $2\theta=10$ ° to 45 ° using a monochromatic $Cu_{K\alpha}$ radiation with a step of 0.04 ° every 12 s. The X-ray diffraction analysis (XRD) analyses are carried out after heat treatment in air atmosphere at 1,000 °C during 15 h to determine the phase composition following the international standard (ISO 13779–3). The procedure consists in calculating the summed intensity ratios of several peaks for each phase. These ratios are compared to those obtained from biphasic standard samples of known percentages. Then, the Ca/P atomic ratio is deduced, considering the percentage of each phase.

Table 2 Corrosion parameters of uncoated Ti6Al4V substrate, electrodeposited HAP coating and electrodeposited Ca-def HAP coating

Physiological solution	Sample	E_{corr} (mV vs SCE)	i_{corr} (μA cm^{-2})
SBF	Ti6Al4V	−308	32
	Ca-def HAP	−99	25
	HAP	−33	7
DMEM	Ti6Al4V	−514	47
	Ca-def HAP	−394	21
	HAP	−321	10
Ringer's solution	Ti6Al4V	−940	89
	Ca-def HAP	−612	74
	HAP	−423	38

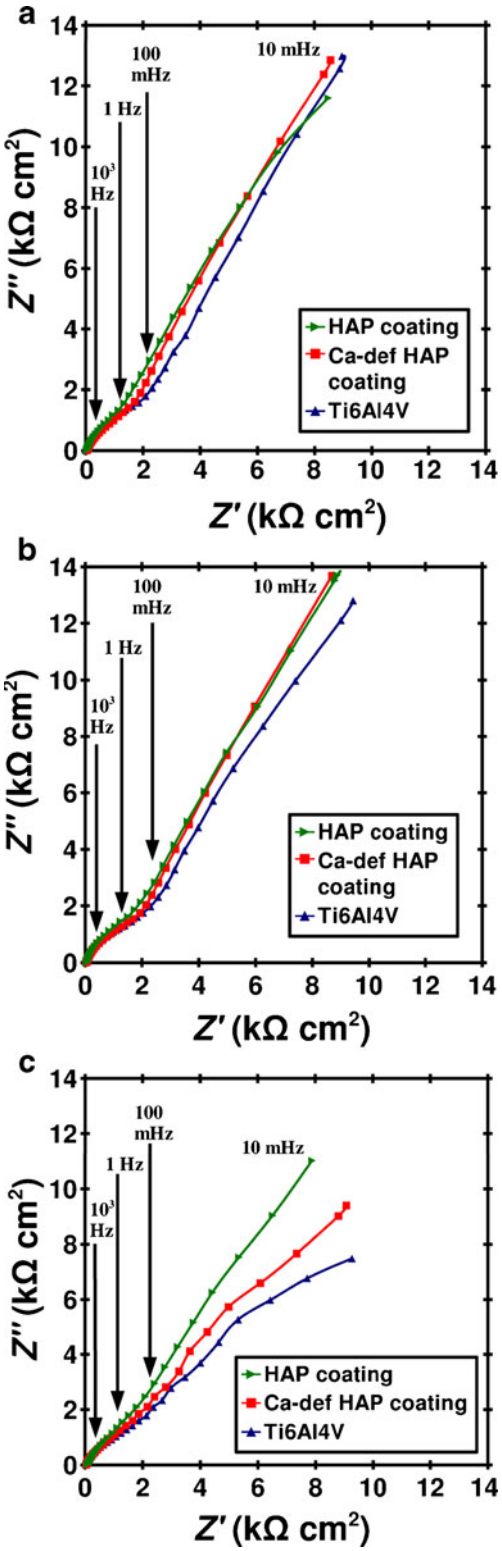

Fig. 4 Nyquist plot of uncoated Ti6Al4V substrate, electrodeposited HAP coating, and electrodeposited Ca-def HAP coating. Measurements are carried out **a** in SBF, **b** in DMEM, and **c** in Ringer's solution

In vitro electrochemical corrosion studies

The protective properties of the coatings are studied using electrochemical methods performed in three different physiological solutions: SBF [40], DMEM [41], and Ringer's solution [42]. SBF and Ringer's solution are saline solutions easily produced in a research laboratory unlike DMEM which contains vitamins and amino acids giving it a

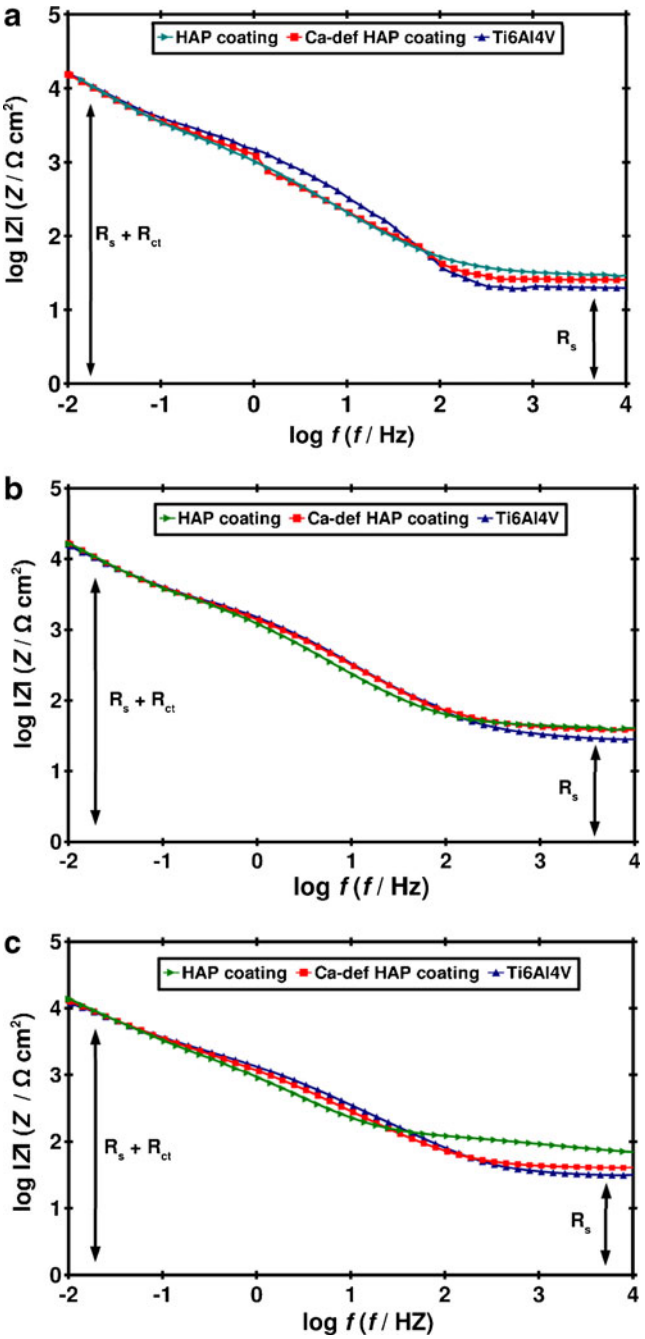

Fig. 5 Bode impedance plot of uncoated Ti6Al4V substrate, electrodeposited HAP coating, and electrodeposited Ca-def HAP coating. Measurements are carried out **a** in SBF, **b** in DMEM, and **c** in Ringer's solution

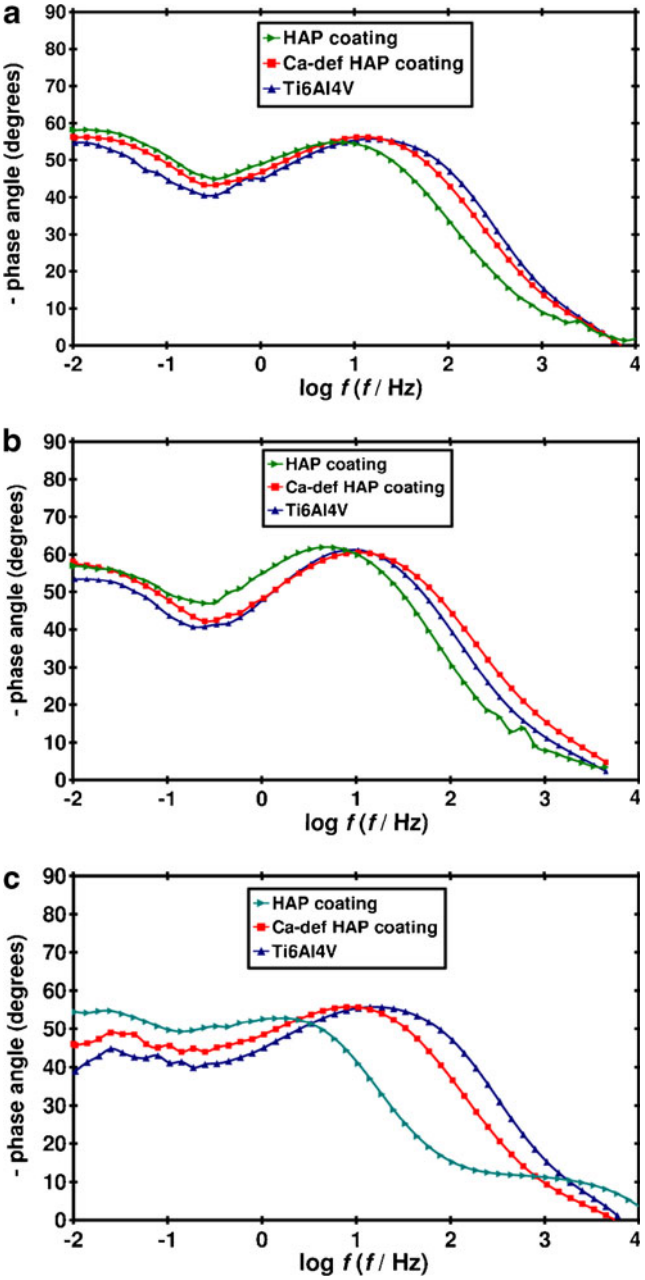

Fig. 6 Bode phase plot of uncoated Ti6Al4V substrate, electrodeposited HAP coating, and electrodeposited Ca-def HAP coating. Measurements are carried out **a** in SBF, **b** in DMEM, and **c** in Ringer's solution

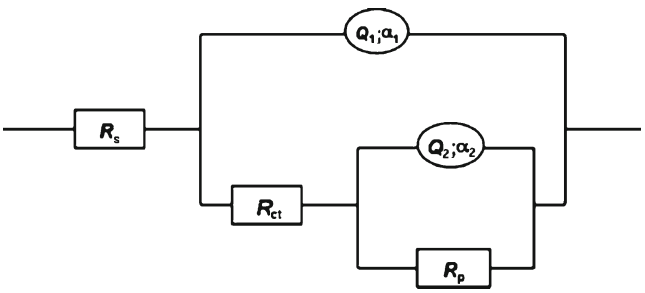

Fig. 7 Equivalent circuit model used for the interpretation of the measured impedance spectra

Table 3 Electrical data extracted from Nyquist plots

	R_s (Ω)	$10^4 \cdot Q_1$	α_1	R_{ct} (kΩ)	$10^4 \cdot Q_2$	α_2	R_p (kΩ)	C_d (μF)	C_F (μF)
Ti6Al4V	39.0±0.4	1.12±0.03	0.801±0.005	3.24±0.16	3.97±0.10	0.760±0.019	84±19	29.0	1,205
Ca-def HAP	28.3±0.2	1.31±0.03	0.771±0.004	3.39±0.14	3.74±0.08	0.794±0.021	99±25	40.0	958
HAP	42.1±0.4	1.63±0.03	0.799±0.005	4.14±0.34	3.52±0.07	0.814±0.020	115±28	46.5	746

composition closer to the human blood plasma. Their chemical compositions are given in Table 1. The temperature is maintained at 37 °C during experiments [43].

Potentiodynamic polarization curves are carried out by increasing the potential at a scan rate of 1.0 mV s^{-1} using a potentiostat/galvanostat instrument (Voltalab PGP 201 Radiometer Analytical—VOLTAMASTER software).

Electrochemical impedance spectra (EIS) measurements are performed at open circuit potential by using a Frequency Response Analyzer (Solartron 1250) monitoring by commercial software (Z-Plot) and coupled to a home-made potentiostat. For the Nyquist and Bode plots, the scan frequency range is set at 10 kHz to 10 mHz with a perturbation amplitude ΔE=10 mV. An equivalent circuit model and impedance parameters are proposed by using the ZView impedance analysis software.

Results and discussion

Physico-chemical characterization of CaP coatings

The SEM micrograph of Fig. 1a shows the morphology of the electrodeposited coating. It reveals that it is composed of small needles and crystallites with apparent porosity. Quantitative analysis from X-ray spectrum of Fig. 1b gives a Ca/P atomic ratio of 1.60 corresponding to a calcium-deficient hydroxyapatite (Ca-def HAP). After heat treatment, the XRD analysis (Fig. 1c) clearly indicates that the coating is composed of two well crystallized phases: the stoichiometric hydroxyapatite (HAP—JCPDS #09-0432) and the β-tricalcium phosphate (β-TCP—JCPDS #09-0169). The calculated percentage of each phase is 52 % for HAP and 48 % for β-TCP. Thus, the corresponding Ca/P atomic ratio is 1.59 in agreement with the value obtained from X-ray microanalysis.

The SEM micrograph of Fig. 2a shows the morphology of the coating synthesized with 9 % H_2O_2 into electrolyte. It clearly shows that this coating is less porous and composed of spheroids formed by the agglomeration of needles. The Ca/P atomic ratio deduced from X-ray microanalysis (Fig. 2b) is 1.67 which corresponds to a stoichiometric hydroxyapatite (HAP: $Ca_{10}(PO_4)_6(OH)_2$). The XRD pattern after heat treatment (Fig. 2c) clearly shows only typical diffraction peaks at 2θ=25.9 °–31.8 °–32.2 °–32.9 °–34 °–39.8 ° corresponding to a well crystallized stoichiometric HAP with Ca/P=1.67.

As described in our previous work [44], the different coating morphologies and compositions are linked to the presence of hydrogen peroxide in the electrolyte. The reduction of hydrogen peroxide during electrolysis leads to higher pH values at the vicinity of the cathode and consequently reduces the calcium deficit of the coating. Moreover, both of these coatings have shown bioactivity properties when they are immersed in physiological solution as their partial dissolution is followed by the precipitation of a bone-like apatite coating [43].

In vitro corrosion measurements

Polarization curves

The Tafel representations of the polarization curves obtained for the uncoated Ti6Al4V substrate, the HAP coating, and the Ca-def HAP coating are plotted in Fig. 3. The

Table 4 Resistance and capacitance values of the equivalent circuit model

Physiological solution	Sample	R_s (Ω)	R_{ct} (kΩ)	R_p (kΩ)	C_d (μF)	C_F (μF)
SBF	Ti6Al4V	30.4	1.92	69.8	11.1	1,706
	Ca-def HAP	31.7	2.54	140.4	24.0	1,503
	HAP	29.2	3.50	154.8	48.9	665
DMEM	Ti6Al4V	39.0	3.24	84.5	29.0	1,205
	Ca-def HAP	28.3	3.39	99.0	40.1	958
	HAP	42.1	4.14	115.2	46.5	746
Ringer's solution	Ti6Al4V	30.4	2.21	35.5	20.0	1,288
	Ca-def HAP	40.3	2.17	83.4	31.6	960
	HAP	36.0	2.89	93.6	35.3	662

measurements are conducted in SBF (Fig. 3a), DMEM (Fig. 3b), and Ringer's solution (Fig. 3c). One may notice that whatever the physiological liquid used, a shift towards nobler potential values is observed in the case of the coated Ti6Al4V samples compared to the uncoated one. This suggests the more passive nature of the calcium phosphate coatings especially when H_2O_2 is introduced into the electrolyte. Moreover, the corrosion parameters deduced from these curves are reported in Table 2. The corrosion potential (E_{corr}) is linked to the thermodynamic stability of the sample immersed in the solution whereas the corrosion current density (i_{corr}) is linked to the kinetics of the corrosion reactions. One may observe that i_{corr} decreases for the coated samples (especially for HAP coating) also indicating an improvement of the corrosion behavior of the prosthetic material. Furthermore, the decrease of these parameters varies with the chemical composition of the physiological liquids as shown by Hsu et al. [45] which have reported the modifications of the corrosion behavior of Ti6Al4V alloy in three physiological body fluid solutions. The differences observed between SBF and Ringer's solution are explained by the higher ionic concentrations of the Ringer's solution, especially of the chloride anion which is known to be a corrosive substance [46]. The DMEM, which contains organic elements, leads to corrosion parameters with intermediate values but significantly different from those obtained in the other media. This indicates that physiological liquids without organic elements are useful to a qualitative study of the corrosion behavior but not for a quantitative study, as highlighted by Bohner et al. [47].

Nevertheless, regardless of the solution, the decreases of i_{corr} and E_{corr} confirm that the calcium phosphate coatings provide a corrosion protection of the Ti6Al4V substrate in physiological solutions particularly with the less porous HAP coating compared to Ca-def HAP coating.

Finally, the results point out that the modulation of the hydrogen peroxide amount modifies the coating porosity and allows choosing the calcium phosphate coating stoichiometry which determines the corrosion behavior of the prosthetic material into physiological medium.

Electrochemical impedance spectroscopy

Figure 4 presents the Nyquist plots of the impedance diagrams measured for the three samples in SBF (Fig. 4a), DMEM (Fig. 4b), and Ringer's solution (Fig. 4c). All of them exhibit a semicircle in the high-frequency region with higher diameters for the coated samples compared to the uncoated one, especially in the case of the HAP coating compared to the Ca-def HAP coating. The Bode plots of the impedance presented in Fig. 5 indicate an increase of the impedance value in the high-frequency domain for the coated substrates. The most important increase is observed in the case of HAP coatings. The Bode

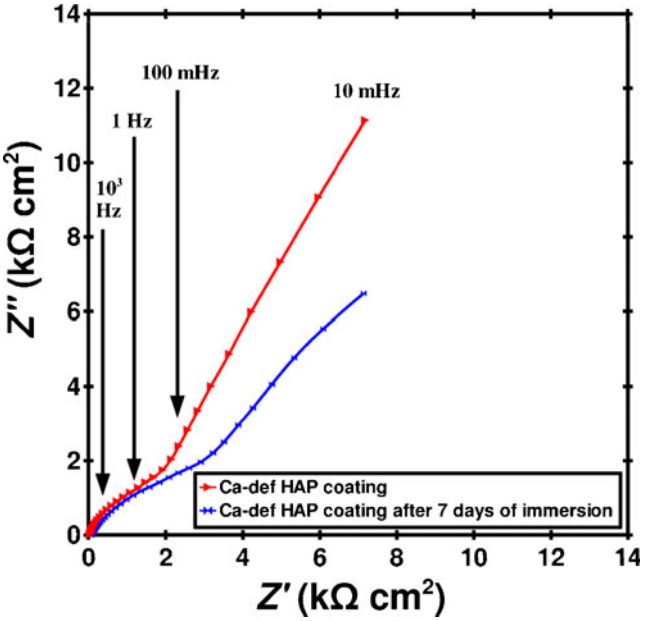

Fig. 8 Nyquist plot of electrodeposited Ca-def HAP coating before and after 7 days of immersion in DMEM

plots of the phase are presented in Fig. 6 where the maximum phase angle observed at low frequencies is characteristic of a capacitive behavior as shown by Advincula et al. [48].

In order to illustrate these results, the Nyquist plots are fitted using the equivalent circuit presented on Fig. 7. It consists of the following elements: a solution resistance R_s which is related to the conductivity of the electrolytic solution; the charge transfer resistance R_{ct} linked to the reaction rate; the polarization resistance R_p of the sample/electrolyte interface; Q_1 and α_1 which are elements linked to the electrical double-layer capacitance C_d; Q_2 and α_2 which are elements linked to the interfacial capacitance C_F highlighting the surface reactions.

Using solid electrodes, the high-frequency loop of the impedance diagram corresponds rarely to the response of a charge transfer resistance in parallel with a purely capacitance but rather, a power-low frequency dependence of capacitance is usually observed. In the equivalent circuit represented in Fig. 7, the constant phase element representation of the double-layer capacitance C_d and the interfacial capacitance C_F have been included. Therefore, the value of C_d and C_F can be obtained respectively through the expression of the high-frequency time constant and the low-

Table 5 Resistance and capacitance values of the equivalent circuit model after 7 days of immersion in DMEM

Sample	R_s (Ω)	R_{ct} (kΩ)	R_p (kΩ)	C_d (μF)	C_F (μF)
Ti6Al4V	26.8	4.31	66.8	13.3	1,710
Ca-def HAP	28.9	6.31	32.3	16.0	1,026
HAP	26.1	9.79	26.7	17.6	764

frequency time constant of the impedance according to the relation established by Brug et al. [49]:

$$C_i = Q_i^{1/\alpha_i} \times \{(1/R_{i-1}) + (1/R_i)\}^{(\alpha_i - 1)/\alpha_i}$$

In the Brug relation $R_s = R_0$, $R_{ct} = R_1$, $R_p = R_2$ and α_1 and α_2 are the dispersion coefficients used to calculate the capacitances of the equivalent circuit. If $\alpha_1 = 1$ then $Q_1 = C_1 = C_d$, and if $\alpha_2 = 1$ then $Q_2 = C_2 = C_F$.

An example of detailed numeric results of the fittings is presented in Table 3 for the three samples immersed in the DMEM solution.

The resistance (R) and capacitance (C) values extracted from the fitted parameters for the three solutions are reported in Table 4. One may observe that for each physiological liquid, the R_s values are of the same order while the charge transfer resistance (R_{ct}) increases for the coated substrates compared to the uncoated one, especially for the HAP coatings. This indicates a decrease of the corrosion rate since the two quantities are inversely proportional [50] and highlights the protective character of the coatings. Similarly, the interfacial capacitance (C_F), a parameter which underlines the electrochemical reactions at the interface [51], decreases when the titanium alloy is coated, especially with HAP. It is noteworthy that these results are in good agreement with the potential corrosion shift observed on the polarization curves of Fig. 3. These results highlight a typical electrochemical behavior of a metallic substrate covered with a porous coating which partially insulates the metal surface [52, 53]. However, the electrolyte penetrates through the pores of the calcium phosphate coating, exposing the metal surface to the corrosive physiological environment. The original electrochemical protocol we developped (pulsed current with or without hydrogen peroxide) allows synthesizing calcium phosphate coatings with various porosity, i.e., with various corrosion behaviors.

Furthermore, we have shown in a recent study [54] that the immersion of Ca-def HAP coatings in DMEM for a long period leads to their partial dissolution, followed by the precipitation of a bone-like apatite layer which modifies the coating thickness, morphology, and porosity. A stability of the process was observed after 7 days of immersion [54]. Thus, in this work, EIS measurements were also conducted after immersion of the samples in DMEM for 7 days. Figure 8 displays the Nyquist plot of this sample compared to the as-deposited coating. The resistance and capacitance values are summarized in Table 5. The main information extracted from these results is the significant increase of the charge transfer resistances (R_{ct}) and the decrease of the double-layer capacitance (C_d), mainly for the coated substrates compared to the uncoated one. These evolutions highlight an improvement of the corrosion protection of the substrate as a function of the dissolution/precipitation process during immersion time. Such behavior is explained by the fact that the precipitated bone-like apatite layer progressively filled the pores in the coating [15, 19]. This surface modification results in a higher resistance to the diffusion of the electroactive species to reach and corrode the metallic substrate. Therefore, the corrosion resistance of the prosthetic material increases with the immersion time in the physiological solution.

Conclusions

In this work, the corrosion behavior of calcium phosphate (CaP)-coated titanium alloy (Ti6Al4V) and uncoated Ti6Al4V has been evaluated by performing polarization and electrochemical impedance spectroscopy (EIS) measurements. An equivalent circuit model has been proposed as an illustration of the electrochemical behavior of the samples. The results indicate that the coatings act as a protective layer and improve the corrosion resistance of the substrate in the three physiological solutions investigated here. According to the original electrochemical process developed, the control of the porosity and the chemical composition of the electrodeposited coating allow governing the corrosion behavior of the prosthetic material in vitro.

References

1. Rack HJ, Qazi JI (2006) Mater Sci Eng C 26:1269–1277
2. He G, Hagiwara M (2006) Mater Sci Eng C 26:14–19
3. Geetha M, Singh AK, Asokamani R, Gogia AK (2009) Prog Mater Sci 54:397–425
4. Barrère F, Mahmood TA, de Groot K, Van Blitterswijk CA (2008) Mater Sci Eng R 59:38–71
5. Mu Y, Kobayashi T, Sumita M, Yamamoto A, Hanawa T (2000) J Biomed Mater Res 49:238–243
6. Guibert G, Irigaray JL, Moretto P, Sauvage T, Kemeny JL, Cazenave A, Jallot E (2006) Nucl Instrum Meth Phys Res 251:246–256
7. Singh R, Dahotre N (2007) J Mater Sci Mater Med 18:725–751
8. Eisenbarth E, Velten D, Müller M, Thull R, Breme J (2002) Biomaterials 25:5705–5713
9. Eisenbarth E, Velten D, Schenk-Meuser K, Linez P, Biehl V, Duschner H, Breme J, Hildebrand H (2002) Biomol Eng 19:243–249
10. Kokubo T, Takadama H (2006) Biomaterials 27:2907–2915
11. Nguyen HQ, Deporter DA, Pilliar RM, Valiquette N, Yakubovich R (2004) Biomaterials 25:865–876
12. Schmidmaier G, Wildemann B, Schwabe P, Stange R, Hoffmann J, Südkamp NP, Haas NP, Raschke M (2002) J Biomed Mater Res B Appl Biomater 63:168–172
13. Sridhar TM, Kamachi Mudali U, Subbaiyan M (2003) Corros Sci 45:2337–2359
14. Pang X, Casagrande T, Zhitomirsky I (2009) J Colloid Interface Sci 330:323–329
15. Souto RM, Laz MM, Reis RL (2003) Biomaterials 24:4213–4221
16. Coelho PG, de Assis SL, Costa I, Thompson VP (2009) J Mater Sci Mater Med 20:215–222

17. Dyshlovenko S, Pateyron B, Pawlowski L, Murano D (2004) Surf CoatTechnol 179:110–117
18. Hesse C, Hengst M, Kleeberg R, Götze J (2008) J Mater Sci Mater Med 19:3235–3241
19. Cabrini M, Cigada A, Rondelli G, Vicentini B (1997) Biomaterials 18:783–787
20. Montazeri M, Dehghanian C, Shokouhfar M, Baradaran A (2011) Appl Surf Sci 257:7268–7275
21. Tkalcec E, Sauer M, Nonninger R, Schmidt H (2001) J Mater Sci 36:5253–5263
22. Metikos-Hukovic M, Tkalcec E, Kwokal A, Piljac J (2003) Surf CoatTechnol 165:40–50
23. Wu C, Ramaswamy Y, Gale D, Yang W, Xiao K, Zhang L, Yin Y, Zreiqat H (2008) Acta Biomater 4:569–576
24. Stoica TF, Morosanu C, Slav A, Stoica T, Osiceanu P, Anastasescu C, Gartner M, Zaharescu M (2008) Thin Solid Films 516:8112–8116
25. Ruban Kumar A, Kalainathan S (2010) Phys B Condens Matter 405:2799–2802
26. Aksakal B, Gavgali M, Dikici B (2010) J Mater Eng Perform 19:894–899
27. Suda Y, Kawasaki H, Ohshima T, Nakashima S, Kawazoe S, Toma T (2006) Thin Solid Films 506:115–119
28. Nelea V, Pelletier H, Mille P, Muller D (2008) Thin Solid Films 453:208–214
29. Corni I, Ryan MP, Boccaccini AR (2008) J Eur Ceram Soc 28:1353–1367
30. Yamaguchi S, Yabutsuka T, Hibino M, Yao T (2008) J Mater Sci Mater Med 19:1419–1424
31. Kwok CT, Wong PK, Cheng FT, Man HC (2009) Appl Surf Sci 255:6736–6744
32. Shirkhanzadeh M (2005) J Mater Sci Mater Med 16:37–45
33. Eliaz N, Eliyahu M (2007) J Biomed Mater Res A 80:621–634
34. Benhayoune H, Laquerriere P, Jallot E, Perchet A, Kilian L, Balossier G, Bubendorff JL, Sockalingum GD (2002) J Mater Sci Mater Med 13:1057–1063
35. Lin S, LeGeros RZ, LeGeros JP (2003) J Biomed Mater Res A 66:819–828
36. Kuo MC, Yen SK (2002) Mater Sci Eng C 20:153–160
37. Eliaz N, Sridhar TM (2008) Cryst Growth Des 8:3965–3977
38. Zhang CY, Zeng RC, Liu CL, Gao JC (2010) Surf CoatTechnol 204:3636–3640
39. Drevet R, Benhayoune H, Wortham L, Potiron S, Douglade J, Laurent-Maquin D (2010) Mater Charact 61:786–795
40. Resende CX, Dille J, Platt GM, Bastos IN, Soares GA (2008) Mater Chem Phys 109:429–435
41. Richard D, Dumelie N, Benhayoune H, Bouthors S, Guillaume C, Lalun N, Balossier G, Laurent-Maquin D (2006) J Biomed Mater Res B 79:108–115
42. Kumar S, Narayanan TSNS (2009) J Alloys Compd 479:699–703
43. Drevet R, Velard F, Potiron S, Laurent-Maquin D, Benhayoune H (2011) J Mater Sci Mater Med 22:753–761
44. Benhayoune H, Drevet R, Faure J, Potiron S, Gloriant T, Oudadesse H, Laurent-Maquin D (2010) Adv Eng Mater 12:B192–199
45. Hsu RWW, Yang CC, Huang CA, Chen YS (2004) Mater Chem Phys 86:269–278
46. Kumar S, Narayanan TSNS (2011) J Appl Electrochem 41:123–820
47. Bohner M, Lemaitre J (2009) Biomaterials 30:2175–2179
48. Advincula MC, Petersen D, Rahemtulla F, Advincula R, Lemons JE (2007) J Biomed Mater Res B Appl Biomater 80:107–120
49. Brug GJ, Ven den Eeden ALG, Sluyters-Rebach M, Sluyters J (1984) J Electroanal Chem 176:275–295
50. Fekry AM, El-Sherif RM (2009) Electrochim Acta 54:7280–7285
51. Luiz de Assis S, Wolynec S, Costa I (2006) Electrochim Acta 51:1815–1819
52. Souto RM, Lemus MM, Reis RL (2004) J Biomed Mater Res A 70:59–65
53. Jamesh M, Kumar S, Narayanan TSNS (2011) J Coat Technol Res. doi:10.1007/s11998-011-9382-6
54. Dumelie N, Benhayoune H, Richard D, Laurent-Maquin D, Balossier G (2008) Mater Charact 59:129–133